High-extinction-ratio silicon polarization beam splitter with tolerance to waveguide width and coupling length variations

Yong Zhang,[1] Yu He,[1] Jiayang Wu,[1] Xinhong Jiang,[1] Ruili Liu,[1] Ciyuan Qiu,[1] Xiaoqing Jiang,[2] Jianyi Yang,[2] Christine Tremblay,[3] and Yikai Su[1,*]

[1]*State Key Lab of Advanced Optical Communication Systems and Networks, Department of Electronic Engineering, Shanghai Jiao Tong University, Shanghai 200240, China*

[2]*Department of Information Science and Electronics Engineering, Zhejiang University, Hangzhou 310027, China*

[3] *Laboratoire de Technologies de Réseaux, École de technologie supérieure, Montreal, Canada*

[*]*yongzhang@sjtu.edu.cn*

Abstract: We demonstrate a compact silicon polarization beam splitter (PBS) based on grating-assisted contradirectional couplers (GACCs). Over 30-dB extinction ratios and less than 1-dB insertion losses are achieved for both polarizations. The proposed PBS exhibits tolerance in width variation, and the polarization extinction ratios remain higher than 20 dB for both polarizations when the width variation is adjusted from + 10 to –10 nm. Benefiting from the enhanced coupling by the GACCs, the polarization extinction ratio can be kept higher than 15 dB and the insertion loss is lower than 2 dB for both polarizations when the coupling length varies from 30.96 to 13.76 μm.

OCIS codes: (230.3120) Integrated optics devices; (230.5440) Polarization-selective devices; (230.7390) Waveguides, planar.

References and links

1. C. Manolatou and H. A. Haus, "High density integrated optics" in *Passive Components for Dense Optical Integration* (Springer, 2002), pp. 97–125.
2. B. Troia, F. De Leonardis, M. Lanzafame, T. Muciaccia, G. Grasso, G. Giannoccaro, C. E. Campanella, and V. Passaro, "Design and optimization of polarization splitting and rotating devices in silicon-on-insulator technology," Adv. Optoelectron. **2014**, 1–16 (2014).
3. L. Yang, R. Ji, L. Zhang, J. Ding, and Q. Xu, "On-chip CMOS-compatible optical signal processor," Opt. Express **20**(12), 13560–13565 (2012).
4. D. Dai, L. Liu, S. Gao, D. X. Xu, and S. He, "Polarization management for silicon photonic integrated circuits," Laser Photonics Rev. **7**(3), 303–328 (2013).
5. H. Guan, A. Novack, M. Streshinsky, R. Shi, Q. Fang, A. E.-J. Lim, G.-Q. Lo, T. Baehr-Jones, and M. Hochberg, "CMOS-compatible highly efficient polarization splitter and rotator based on a double-etched directional coupler," Opt. Express **22**(3), 2489–2496 (2014).
6. D. Dai, "Silicon polarization beam splitter based on an asymmetrical evanescent coupling system with three optical waveguides," J. Lightwave Technol. **30**(20), 3281–3287 (2012).
7. Y. Ding, L. Liu, C. Peucheret, and H. Ou, "Fabrication tolerant polarization splitter and rotator based on a tapered directional coupler," Opt. Express **20**(18), 20021–20027 (2012).
8. Z. Su, E. Timurdogan, E. S. Hosseini, J. Sun, G. Leake, D. D. Coolbaugh, and M. R. Watts, "Four-port integrated polarizing beam splitter," Opt. Lett. **39**(4), 965–968 (2014).
9. L. Liu, Y. Ding, K. Yvind, and J. M. Hvam, "Efficient and compact TE-TM polarization converter built on silicon-on-insulator platform with a simple fabrication process," Opt. Lett. **36**(7), 1059–1061 (2011).
10. A. Xie, L. Zhou, J. Chen, and X. Li, "Efficient silicon polarization rotator based on mode-hybridization in a double-stair waveguide," Opt. Express **23**(4), 3960–3970 (2015).
11. L. Chen, C. R. Doerr, and Y.-K. Chen, "Compact polarization rotator on silicon for polarization-diversified circuits," Opt. Lett. **36**(4), 469–471 (2011).
12. G. F. R. Chen, T. Wang, K. J. A. Ooi, A. K. L. Chee, L. K. Ang, and D. T. H. Tan, "Wavelength selective mode division multiplexing on a silicon chip," Opt. Express **23**(6), 8095–8103 (2015).
13. D. Po, L. Xiang, S. Chandrasekhar, L. L. Buhl, R. Aroca, and C. Young-Kai, "Monolithic silicon photonic integrated circuits for compact 100 + Gb/s coherent optical receivers and transmitters," IEEE J. Sel. Top. Quantum Electron. **20**(4), 150–157 (2014).
14. B. Shen, P. Wang, R. Polson, and R. Menon, "An integrated-nanophotonics polarization beamsplitter with 2.4×2.4 μm^2 footprint," Nat. Photonics **9**(6), 378–382 (2015).

#257485 Received 26 Jan 2016; revised 5 Mar 2016; accepted 11 Mar 2016; published 16 Mar 2016

15. B. Rahman, N. Somasiri, C. Themistos, and K. Grattan, "Design of optical polarization splitters in a single-section deeply etched MMI waveguide," Appl. Phys. B **73**(5), 613–618 (2001).
16. Y. Ding, H. Ou, and C. Peucheret, "Wideband polarization splitter and rotator with large fabrication tolerance and simple fabrication process," Opt. Lett. **38**(8), 1227–1229 (2013).
17. X. Ao, L. Liu, L. Wosinski, and S. He, "Polarization beam splitter based on a two-dimensional photonic crystal of pillar type," Appl. Phys. Lett. **89**(17), 171115 (2006).
18. J. Feng and Z. Zhou, "Polarization beam splitter using a binary blazed grating coupler," Opt. Lett. **32**(12), 1662–1664 (2007).
19. H.-S. Chu, E.-P. Li, P. Bai, and R. Hegde, "Optical performance of single-mode hybrid dielectric-loaded plasmonic waveguide-based components," Appl. Phys. Lett. **96**(22), 221103 (2010).
20. X. Guan, H. Wu, Y. Shi, and D. Dai, "Extremely small polarization beam splitter based on a multimode interference coupler with a silicon hybrid plasmonic waveguide," Opt. Lett. **39**(2), 259–262 (2014).
21. D. Dai and J. E. Bowers, "Novel ultra-short and ultra-broadband polarization beam splitter based on a bent directional coupler," Opt. Express **19**(19), 18614–18620 (2011).
22. D. Dai, Z. Wang, and J. E. Bowers, "Ultrashort broadband polarization beam splitter based on an asymmetrical directional coupler," Opt. Lett. **36**(13), 2590–2592 (2011).
23. D. W. Kim, M. H. Lee, Y. Kim, and K. H. Kim, "Planar-type polarization beam splitter based on a bridged silicon waveguide coupler," Opt. Express **23**(2), 998–1004 (2015).
24. H. Qiu, Y. Su, P. Yu, T. Hu, J. Yang, and X. Jiang, "Compact polarization splitter based on silicon grating-assisted couplers," Opt. Lett. **40**(9), 1885–1887 (2015).
25. Y. Zhang, Y. He, J. Wu, R. Liu, C. Qiu, and Y. Su, " High-extinction-ratio and fabrication-tolerant polarization beam splitter based on grating-assisted contradirectional couplers," in *Optical Fiber Communication Conference* (Optical Society of America, 2016), paper Tu3E.2.
26. D. Taillaert, P. Bienstman, and R. Baets, "Compact efficient broadband grating coupler for silicon-on-insulator waveguides," Opt. Lett. **29**(23), 2749–2751 (2004).
27. H. Qiu, H. Yu, T. Hu, G. Jiang, H. Shao, P. Yu, J. Yang, and X. Jiang, "Silicon mode multi/demultiplexer based on multimode grating-assisted couplers," Opt. Express **21**(15), 17904–17911 (2013).
28. H. Fukuda, K. Yamada, T. Tsuchizawa, T. Watanabe, H. Shinojima, and S. Itabashi, "Ultrasmall polarization splitter based on silicon wire waveguides," Opt. Express **14**(25), 12401–12408 (2006).

1. Introduction

Silicon nanowire waveguides with high index-contrast between core and cladding generally have high birefringence values, which result in polarization mode dispersion and polarization dependent loss [1–3]. Polarization handling devices [4,5], such as polarization beam splitters (PBSs) [6–8] and polarization rotators [9–11], are important components in polarization-diversity schemes to eliminate the polarization sensitivities [12,13].

A PBS is a key component for splitting or combining two orthogonal polarization modes [14]. Many schemes were proposed to realize PBS devices, including multimode interference (MMI) structures [15,16], photonic crystal [17], out-of-plane grating [18], hybrid plasmonic waveguides [19,20], directional couplers (DCs) [21,22] and so on. Polarization extinction ratios (PERs) of previously reported PBSs were below 30 dB, except for the DC-based device in [10]. However, the optical coupling between two waveguides in the DC-based PBS was periodically dependent on the coupling length and sensitive to fabrication variations. The PER of the DC-based PBS decreased from 20 dB to 12 dB as the coupling length varied from 6.5 μm to 5.5 μm [23]. A compact PBS based on asymmetrical grating-assisted contradirectional couplers (GACCs) was theoretically proposed [24]. An advantage of such PBS is that it does not require stringent phase matching and coupling length conditions. Recently, we fabricated such a GACC-based PBS and presented preliminary experimental results [25].

In this paper, we perform a detailed study of a high-extinction-ratio PBS in terms of design, fabrication, and tolerance to width and coupling length variations. The device is fabricated on a silicon-on-insulator (SOI) wafer with a total length of < 30 μm. The TE mode coupling between the two waveguides is strongly enhanced by GACCs, while the TM coupling does not occur. In theory the optical coupling between the two waveguides is monotonically dependent on the coupling length. To realize a single etch and simple fabrication process, a symmetrical vertical structure is used in our design, which differs from that in [24]. The upper cladding of both waveguides is air. The PERs of the fabricated PBS are higher than 30 dB for both polarizations in a wavelength range of 20 nm. When the width varies from + 10 to –10 nm, the PERs of the PBSs are > 20 dB for both polarizations. As the coupling length varies from 30.96 μm to 13.76 μm, the PERs remain higher than 15 dB for

#257485 Received 26 Jan 2016; revised 5 Mar 2016; accepted 11 Mar 2016; published 16 Mar 2016

both polarizations. To the best of our knowledge, our device achieves record high PERs with large tolerance in waveguide width and coupling length variations.

2. Device design and fabrication

Figures 1(a) and (b) depicts a 3D and top view of the schematic configuration for the proposed PBS based on a GACC structure, respectively. The device consists of two parallel silicon strip waveguides, A and B. The bent waveguide and S-bend at the Input and Cross ports, respectively, are used to separate the two waveguides. The corrugations on the sidewall of the two waveguides are designed to form grating structures. The GACC is designed to enhance the coupling of the TE mode, but has no effect on the coupling of the TM mode. The phase-matching condition is satisfied for the coupling of the TM mode, but not for the coupling of the TE mode. Therefore, a TE-polarized light is contra-directionally coupled from waveguide A to waveguide B by the periodic corrugations. High-efficiency TE-polarized light output is obtained in the Cross port. A TM-polarized light goes through waveguide A without coupling. High-efficiency TM-polarized light output is obtained in the Thru port. Thus, the TE- and TM- polarized light signals are separated by the GACCs. It is noted that the asymmetrical configuration in on-plane direction can suppress the co-directional coupling between the waveguides. A symmetrical structure in the vertical direction is used in our design to realize a single etch and simple fabrication process.

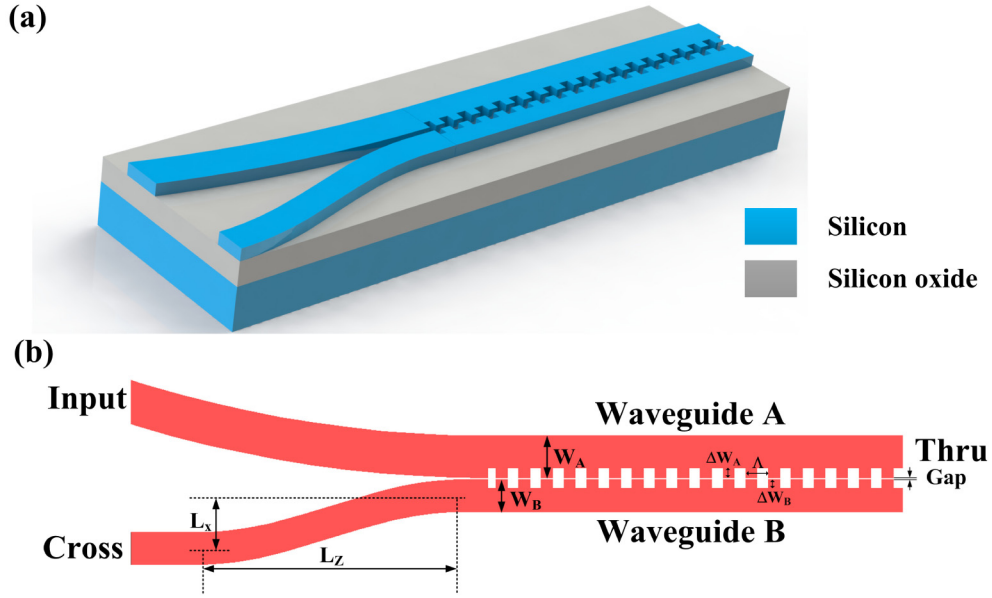

Fig. 1. The schematic configuration of the proposed PBS based on a GACC structure, (a) the 3D view, (b) the top view.

The thickness of the silicon waveguides in the PBS structure is 220 nm. The radius of the bent waveguide at the Input port is 18 μm, which is large enough to ensure low-loss for TM-polarized light. The widths of the waveguides are W_A = 600 nm and W_B = 450 nm, respectively. The period of the corrugations is Λ = 344 nm. The duty cycle of the corrugations is 52%. The corrugation widths on waveguide A and waveguide B are ΔW_A = 137 nm and ΔW_B = 123 nm, respectively. The gap between the waveguides is 65 nm. The S-bend at the Cross port is designed to separate the input and cross waveguides. The offsets for the S-bend are L_x = 0.8 μm and L_z = 4 μm. The coupling length of the two waveguides is determined by the period Λ and corrugation period numbers N. The input waveguide A has a width of 600 nm, which is a multimode waveguide for the TE polarization. Adiabatic tapers are used for coupling to a narrower single-mode waveguide at the input and output ports. The proposed

#257485 Received 26 Jan 2016; revised 5 Mar 2016; accepted 11 Mar 2016; published 16 Mar 2016

PBSs also work well if the devices are covered with dielectric upper cladding. The feature sizes are compatible with standard processing in silicon photonics foundries, expect for the gap of 65 nm. A larger gap may be used for fabrication using deep ultraviolet lithography, but it results in a slightly longer coupling length.

The three-dimensional finite-difference time-domain (3D FDTD) method is applied to simulate the proposed structure (N = 60). Note that the radius of the bent waveguide at the Input port is reduced to 5 μm to decrease the calculation time in the simulation. The simulated power distributions for the TE- and TM- polarized light inputs are shown in Figs. 2(a) and (b), respectively. When the TE-polarized light is injected into the Input port, the optical signal is contra-directionally coupled to the cross waveguide and outputs from the Cross port, while, for the TM-polarized input, the optical signal goes directly through waveguide A and outputs from the Thru port. The TE- and TM- polarized light signals are separated by the GACC structure. Weak co-directional coupling between the two waveguides is observed for the TM-polarized light. We attribute it to the symmetrical structure in the vertical direction.

In the experiment, the GACC-based PBSs were fabricated on a SOI wafer (220-nm-thick silicon on 3000-nm-thick silica). E-beam lithography (Vistec EBPG 5200) was used to define the structures on the ZEP520A resist. Then the patterns were transferred to the top silicon layer by inductively coupled plasma (ICP) dry etching using SF_6 and C_4F_8 gases. Scanning electron microscope (SEM) images of the fabricated GACC-based PBS with corrugation period numbers N = 80 are shown in Fig. 3.

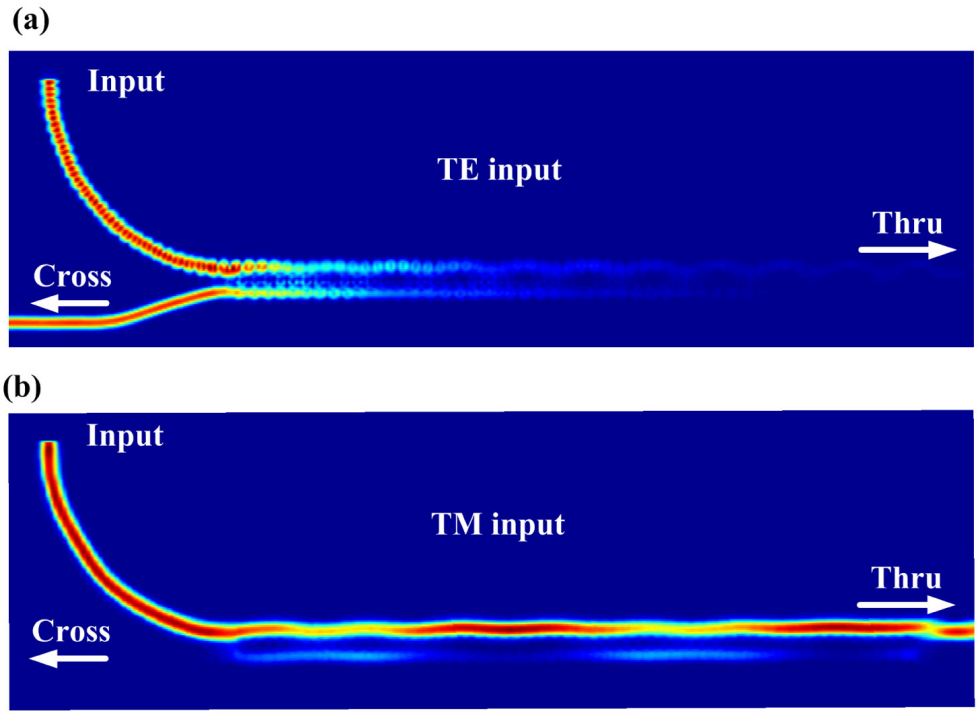

Fig. 2. The simulated power distributions for (a) TE- polarized light inputs, (b) TM- polarized light inputs.

In the measurements, the TE- and TM- polarized lights from a tunable laser (Keysight 81960A) were coupled into/out of the chip by grating couplers. The output spectra were recorded by an optical spectrum analyzer (OSA) (Yokogawa AQ6370B). The grating couplers exhibit a significant polarization dependence [26]. The period of the TE gratings is 630 nm, and the filling factor is 50%. And that for the TM gratings are 1080 nm and 48%, respectively. The etching height of both gratings is 70 nm. The coupling losses of the TE- and

#257485 Received 26 Jan 2016; revised 5 Mar 2016; accepted 11 Mar 2016; published 16 Mar 2016

TM- polarized grating couplers were 7.7 dB/port and 8.7 dB/port at the central wavelengths of the gratings, respectively. Two identical PBSs were fabricated to measure responses for the TE- and TM- polarized lights inputs, respectively.

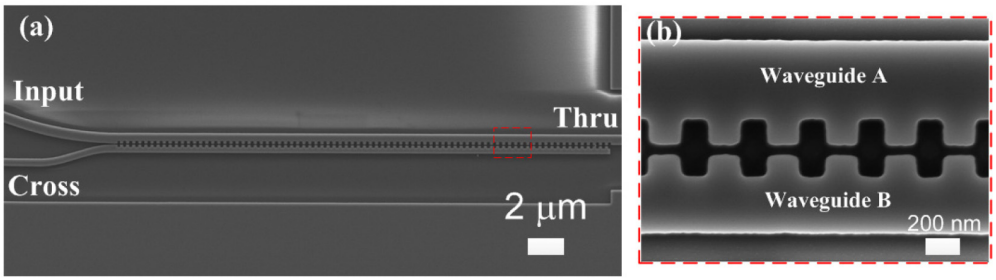

Fig. 3. (a) SEM image of the fabricated GACC-based PBS with corrugations period number N = 80. (b) Magnified micrograph of the GACC.

3. Results and discussion

Figure 4 illustrates the measured transmission responses at the Cross and Thru ports of the fabricated PBS for the TE- and TM- polarized input signals, respectively. The corrugation period numbers N is 80, and the corresponding coupling length is 27.52 μm. The responses are normalized to the transmission of a grating-coupled straight waveguide. For the TE-polarized light input, the PER is higher than 30 dB in the wavelength range of 1517 ~1538 nm, and the insertion loss is < 1 dB. For the TM-polarized light input, the PER is higher than 30 dB in the wavelength range of 1517 ~1544 nm, and the insertion loss is < 1 dB. Some noise observed in Fig. 4 is attributed to that the received power is close to the detection limit of the OSA. The operation wavelength can be finely tuned by changing the corrugation period and the width. Broader operation bandwidth could be realized by appling larger refractive-index perturbation and stronger coupling [23].

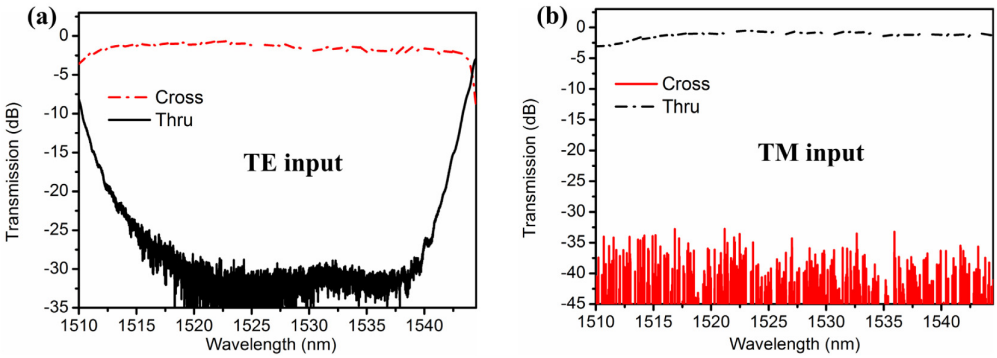

Fig. 4. Measured transmission responses at the Cross and Thru ports for (a) TE-polarization and (b) TM-polarization. The corrugation period numbers N and coupling length of the fabricated PBS are 80 and 27.52 μm, respectively.

Generally, inevitable errors occur in the device fabrication process and degrade the device performance. The variations in waveguide dimensions introduced by design or fabrication imperfections lead to phase mismatch and affect the cross-coupling ratio [7,16,23]. To measure the transmission sensitivity of the device to waveguide dimensions, PBSs with waveguide width variations of $\Delta w = \pm 10$ nm for both waveguides A and B were fabricated. The measured transmission responses for the fabricated PBSs with width variations of $\Delta w = +10$ nm and $\Delta w = -10$ nm are shown in Figs. 5(a) and (b), respectively. The corrugation period numbers N is 70, and the coupling length L_c is 24.08 μm. For a width variation Δw of + 10 nm, the PERs remain higher than 20 dB for both polarizations in the wavelength range of

#257485 Received 26 Jan 2016; revised 5 Mar 2016; accepted 11 Mar 2016; published 16 Mar 2016

1515 ~1536 nm, and the corresponding insertion losses are < 2 dB. While in the case of Δw = –10 nm, the PERs are > 20 dB for both polarizations in the wavelength range of 1510 ~1529 nm, and the corresponding insertion losses are < 1 dB. The experimental results of the reference device with N = 70 and Δw = 0 nm are shown in Fig. 6(b). These results verify that the presented PBSs are tolerant to width variations.

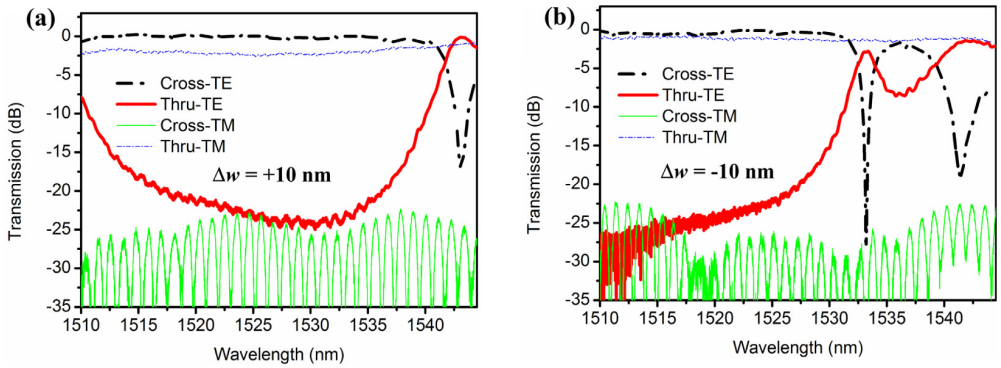

Fig. 5. Measured transmission responses at the Cross and Thru ports for TE- and TM-polarizations of the fabricated PBSs with width variations of (a) Δw = + 10 nm and (b) Δw = – 10 nm.

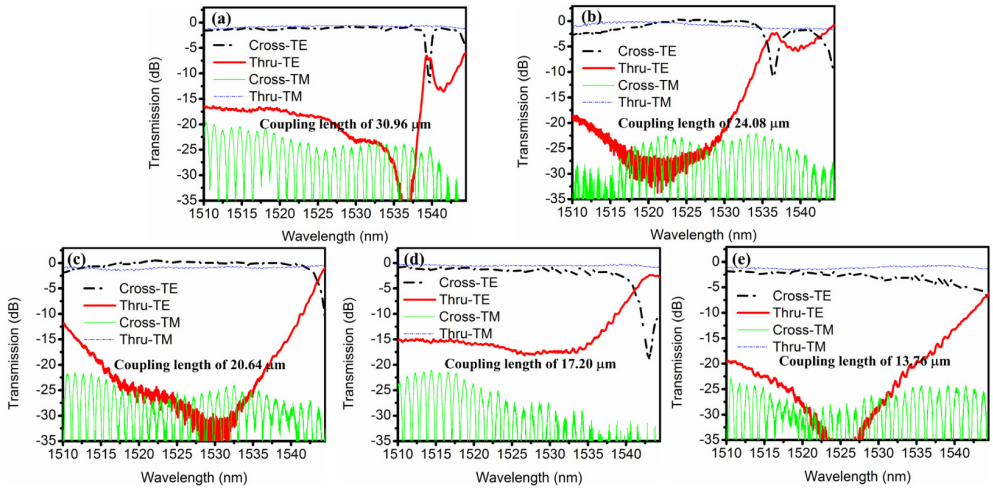

Fig. 6. Measured transmission responses at the Cross and Thru ports for TE- and TM-polarizations of the fabricated PBSs with (a) corrugation period number N = 90, coupling length L_C of 30.96 μm, (b) N = 70, L_C = 24.08 μm, (c) N = 60, L_C = 20.64 μm, (d) N = 50, L_C = 17.02 μm, (e) N = 40, L_C = 13.76 μm.

The gap between the two waveguides and the corrugation width are important parameters in the design of the GACCs. However, if the coupling length is long enough, these parameters have little effect on the mode transitions [24,27]. To evaluate the effect of the coupling length on the performance of the GACCs, PBSs with different coupling lengths were fabricated. The measured responses for the fabricated PBSs with coupling lengths L_c of 30.96, 24.08, 20.64, 17.02 and 13.76 μm are shown in Figs. 6(a)-(e), respectively. In Fig. 6(a), the PERs are higher than 17 dB and 20 dB in the wavelength range of 1510 ~1537 nm for the TE- and TM-polarized lights, respectively. The corresponding insertion losses are < 2 dB for both polarizations. In the case of L_c = 24.08 μm shown in Fig. 6(b), the PERs are higher than 20 dB in the wavelength range of 1513 ~1530 nm for the TE- and TM- polarized lights, respectively, and the insertion losses are < 2 dB for both polarizations. For the PBS with a coupling length

#257485 Received 26 Jan 2016; revised 5 Mar 2016; accepted 11 Mar 2016; published 16 Mar 2016

of 20.64 μm in Fig. 6(c), the PERs remain higher than 20 dB for both polarizations in the wavelength range of 1515 ~1537 nm, and the insertion losses are < 1 dB. In Fig. 6(d), the PERs are higher than 15 dB and 20 dB in the wavelength range of 1510 ~1535 nm for the TE- and TM- polarized lights, respectively, and the insertion losses are < 2 dB and < 1 dB for the TE- and TM- polarized lights, respectively. If the coupling length decreases to 13.76 μm as depicted in Fig. 6(e), the PERs remain higher than 20 dB for both polarizations in the wavelength range of 1510 ~1533 nm, and the corresponding insertion losses are < 2 dB. These results show that, as the coupling length varies from 30.96 μm to 13.76 μm, the PERs still remain higher than 15 dB and the insertion losses are lower than 2 dB for both polarizations, which demonstrates that the PBSs are insensitive to coupling length variations. The PERs of the device with N = 90 are lower than those of the device with N = 80 in the experiment, as shown in Fig. 6. We attribute it to the imperfection introduced in the fabrication.

As the coupling of the device is enhanced by the GACCs, the optical coupling between the two waveguides and the PERs are monotonically dependent on the coupling length in theory. Longer length may not improve PERs noticeably, at the cost of increased device footprint. For a trade-off coupling length of 27.52 μm, the PERs are higher than 30 dB.

To investigate the fabrication tolerance, we simulated the PERs of the devices with different silicon thicknesses and corrugation widths by 3D-FDTD method, respectively. The simulated results of the PBSs with silicon thicknesses of 215, 220 and 225 nm are shown in Fig. 7(a). The PERs of the devices with different corrugation widths are depicted in Fig. 7(b). The PERs do not experience significant degradations as the silicon thickness and corrugation width change.

Table 1 compares our device with various state-of-the-art silicon PBSs. It indicates that, our GACC-based PBSs have the largest PERs and are tolerant to waveguide width and coupling length variations.

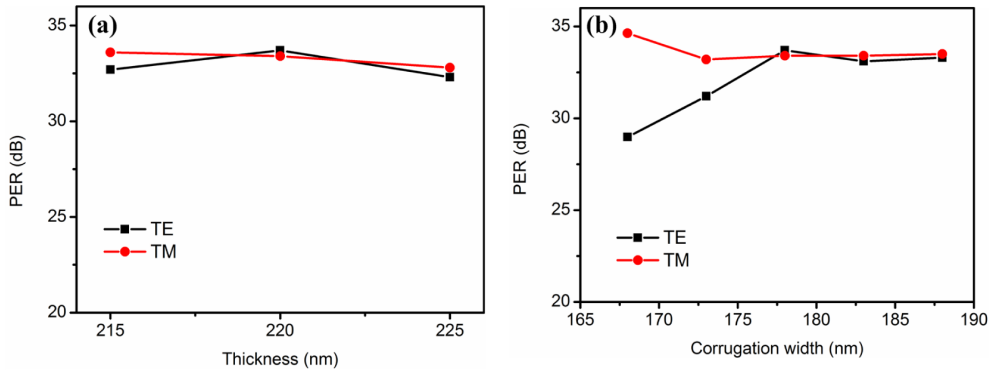

Fig. 7. Simulated PERs of the devices with (a) different silicon thicknesses and (b) different corrugation widths.

#257485 Received 26 Jan 2016; revised 5 Mar 2016; accepted 11 Mar 2016; published 16 Mar 2016

Table 1. Comparisons of Various Silicon Polarization Beam Splitters

Structures	PER (dB)	Insertion loss (dB)	Operation bandwidth (nm)	Tolerance
Double-etched directional coupler [5]	20	< 0.5	30	–
Mode-evolution-based PBS [8]	10	< 3.5	150	–
Nonlinear-search-algorithm-based PBS [14]	10	–	32	± 20 nm for silicon thickness
MMI-based PSR [16]	12	< 2.5	100	50 nm for width
Bent directional coupler [21]	10	< 1	80 nm @ PER > 6 dB	± 20 nm for width
Bridged directional coupler [23]	< 23	< 2.1	80	± 10 nm for width; 6.5 ~8.5 μm for length
Directional coupler [28]	15	0.5	50	–
GACC-based PBS (our device)	30	< 1	21	± 10 nm for width; 13.76 ~30.96 μm for coupling length

4. Summary

In conclusion, we have experimentally demonstrated a compact silicon PBS based on GACCs. The PBSs are realized by a simple single etch fabrication process. The PERs and insertion losses of the fabricated PBSs are > 30 dB and < 1 dB, respectively, for both polarizations in a wavelength range of 20 nm. For width variations ranging from + 10 nm to – 10 nm, the PERs and insertion losses of the PBSs remain higher than 20 dB and lower than 2 dB for both polarizations in a wavelength range of 20 nm. Due to the coupling enhanced by the GACCs, the coupling length does not need rigorous control. The PERs remain higher than 15 dB and the insertion losses are lower than 2 dB for both polarizations as the coupling length varies from 30.96 μm to 13.76 μm. These results indicate that the demonstrated PBSs are tolerant to waveguide width and coupling length variations, enabling fabrication-tolerant mass production of the PBS devices.

Acknowledgments

This work was supported in part by the 863 High-Tech Program under Grant 2015AA017001, in part by the National Natural Science Foundation of China (NSFC) under Grant 61235007 and 61505104, and in part by the Natural Science Foundation of Shanghai under Grant 15ZR1422800. We thank the Center for Advanced Electronic Materials and Devices (AEMD) for the support in device fabrications.

#257485 Received 26 Jan 2016; revised 5 Mar 2016; accepted 11 Mar 2016; published 16 Mar 2016